

1 **Estimating χ using fast-response thermistors on traditional shipboard**

2 **CTDs: sources of uncertainty and bias.**

3 Andy Pickering*

4 *College of Earth, Ocean, and Atmospheric Sciences, Oregon State University, Corvallis, OR.*

5 Jonathan Nash

6 *College of Earth, Ocean, and Atmospheric Sciences, Oregon State University, Corvallis, OR.*

7 James N Moum

8 *College of Earth, Ocean, and Atmospheric Sciences, Oregon State University, Corvallis, OR.*

9 Jen MacKinnon

10 *UCSD / Scripps Institute of Oceanography*

11 *Corresponding author address: College of Earth, Ocean, and Atmospheric Sciences, Oregon State
12 University, Corvallis, OR.

13 E-mail:

ABSTRACT

14 The acquisition of turbulence data from traditional shipboard CTD casts is 
15 attractive, as it has the potential to significantly increase the amount of deep-
16 ocean mixing observations globally. While data from shear-probes are eas-
17 ily contaminated by motion of the instrument platform, the measurement of
18 temperature gradient is relatively insensitive to vehicle vibration, making it
19 possible to measure temperature gradient from a shipboard CTD rosette. The
20 purpose of this note is to investigate the error and bias in estimating the rate
21 of dissipation of temperature variance χ and turbulent diffusivity K_T from
22  thermistors mounted on traditional CTD casts. The most significant source
23 of error is associated with the fact that fast-response FP07 thermistors resolve
24 only a fraction of the temperature gradient variance at the fallspeed of typi-
25 cal CTD casts. Assumptions must be made about the wavenumber extent of
26 the temperature gradient spectrum, which scales with the rate of dissipation
27 of turbulent kinetic energy, a quantity that is not directly measured. Here we
28 utilize observations from a microstructure profile  to demonstrate the validity
29 of our method of estimating χ from thermistor data, and to assess uncertainty
30 and bias. We then apply this methodology to temperature gradient profiles ob-
31 tained from χ pods mounted on a CTD (the CTD- χ pod), and compare these
32 to microstructure profiles obtained almost synoptically at the equator. CTD-
33 χ pod estimates of χ compare favorably to the direct microstruc-ture measure-
34 ments and demonstrate that the χ pod method is not significantly biased. This
35 supports the utility of the measurement as part of the global repeat hydrog-
36 raphy program (GO-SHIP) cruises, during which this type of data has been
37 acquired during the past few years.

³⁸ **1. Introduction**

³⁹ Turbulent mixing affects the distribution of heat, salt, and nutrients throughout the global ocean.

⁴⁰ Diapycnal mixing of cold, dense water with warmer water above maintains the abyssal overturning

⁴¹ circulation (Munk 1966; Munk and Wunsch 1998), which affects global climate. Because the

⁴² turbulence that drives mixing generally occurs at scales that are not resolved in climate models,

⁴³ it must be parameterized, based on either (i) aspects of the resolved model dynamics, (ii) through

⁴⁴ higher resolution models that capture the dynamics that feed energy to turbulence, or (iii) using

⁴⁵ other parameterizations that either dynamically or statistically quantify turbulent fluxes. Recent

⁴⁶ investigations have demonstrated that these models are sensitive to the magnitude and distribution

⁴⁷ of mixing (Melet et al. 2013). A comprehensive set of measurements that spans relevant dynamical

⁴⁸ regimes is needed to constrain mixing and develop more accurate parameterizations.

⁴⁹ Direct measurement of mixing with microstructure profilers equipped with shear probe wells⁵⁰ well-

⁵¹ suited for targeting upper-ocean processes. However, this technique can be expensive, time-

⁵² intensive, and requires considerable care and expertise. Moreover, tethered profilers can't reach

⁵³ abyssal depths, requiring autonomous instruments to get deeper than ~1000-2000 m. As a result,

⁵⁴ existing measurements of diapycnal mixing, especially in the deep ocean, are sparse (Waterhouse

⁵⁵ et al. 2014). In order to obtain a larger quantity of mixing estimates, considerable work has gone

⁵⁶ into inferring mixing from measurements of the outer scales of turbulence, which are easier to

⁵⁷ obtain. One popular method is the use of Thorpe scales, where diapycnal mixing is inferred from

⁵⁸ inversions in profiles of temperature or density (Thorpe 1977; Dillon 1982). The size of resolvable

⁵⁹ overturn is limited by the profiling speed and instrument noise (Galbraith and Kelley 1996). While

⁶⁰ some studies indicate relatively good agreement with microstructure and other observations, there

remain questions about the general validity of the method and the assumptions made (Mater et al.

61 2015; Scotti 2015). Parameterizations based on profiles of shear and/or strain have also been de-
62 veloped and applied to estimate diapycnal mixing (Gregg 1989; Kunze et al. 2006; Polzin et al.
63 2013; Whalen et al. 2012, 2015). However, they rely on a series of assumptions about the cascade
64 of energy from large to small scales that are often violated; numerous studies (i.e., Waterman et al.
65 (2013)) have shown that there is significant uncertainty associated with these parameterizations, in
66 that there can be a consistent bias in a particular region, yet the sense of the bias (i.e., overpredict
67 vs. underpredict) is not known a priori.

68 Quantifying turbulence from velocity shear variance (to compute the dissipation rate of turbu-
69 lent kinetic energy ε) is challenging on moorings or profiling platforms because there is usually
70 too much vibration and/or package motion for shear-probes to be useful. Pitot-static tubes have
71 recently been used for this purpose, plus providing independent measurements of speed (Moum
72 2015). Other methods (i.e., optics or acoustics) may hold some promise, but lack of scatterers
73 often precludes this type of measurement, especially in the abyss. In addition, shear probes only
74 provide ε , not the mixing of scalars, K , which is often inferred from ε by assuming a mixing
75 efficiency Γ (Osborn 1980) as $K = \Gamma\varepsilon/N^2$, where N^2 is the buoyancy frequency. A more direct
76 measure of turbulent mixing is obtained from the dissipation rate of temperature variance χ (Os-
77 born and Cox 1972). This has the advantage that (i) the temperature and temperature gradient can
78 be computed and are relatively straightforward to measure, and (ii) the estimation of mixing from
79 χ does not require assumptions about Γ . However, the spectrum of temperature gradient extends
80 to very small scales, so that its spectrum is seldom fully resolved (and unlike shear variance, the
81 wavenumber extent of the temperature gradient spectrum does not scale with its amplitude, but
82 instead depends on ε). Assumptions about the spectral shape (Kraichnan vs. Batchelor, and the
83 value of the “constant” q) and its wavenumber extent (governed by the Batchelor wavenumber
84 $k_b = [\varepsilon/(vD_T^2)]^{1/4}$ (Batchelor 1959)) are thus necessary to determine χ unless measurements cap-

ture the full viscous-diffusive subrange of turbulence (i.e., down to scales $\Delta x \sim 1/k_b \sim 1\text{mm}$),
a criterion seldom achieved. To resolve this, we follow Alford and Pinkel (2000) and Moum
and Nash (2009) and make the assumption that $K_T = K_p$ to determine the dissipation rate as
 $\varepsilon_\chi = (N^2 \chi) / (2\Gamma \langle dT/dz \rangle^2)$, permitting estimation of k_b .

The goal of this paper is to outline and validate the methods used to compute χ and K_T with
 χ pods mounted on CTDs (Figure 1). We do this by applying our processing methodology to pro-
files of temperature gradient measured by thermistors on the ‘Chameleon’ microstructure profiler,
which provides a direct test of our methodology. Because Chameleon is a loosely tethered pro-
filer equipped with shear probes (Moum et al 1995), it directly measures ε and allows us to test
our assumptions. Specifically, it allows us to determine biases associated with computing χ from
partially-resolved temperature gradient spectra alone, as compared to computation that includes ε ,
which constrains the wavenumber extent of the scalar spectra. After establishing that the method
works, we then compare CTD- χ pod profiles to nearby microstructure profiles.

2. Data

a. EQ14



Data were collected on the R/V Oceanus in Fall 2014 during the EQ14 experiment to study
equatorial mixing. More than 2700 Chameleon profiles were made, along with 35 CTD- χ pod
profiles bracketed by Chameleon profiles in order to maintain calibrations during the cruise. Most
Chameleon profiles were made to a maximum depth of about 250m, with CTD casts going to
500m or deeper. The EQ14 experiment and results are discussed in more detail in (SJ Warner, RN
Holmes, EH McHugh-Hawkins, JN Moum, 2016: Buoyant gravity currents released from tropical
instability waves, JPO, in preparation) and Holmes et al. (2016).

107 **3. Methods**

108 As mentioned in the introduction, the temperature gradient spectrum is rarely fully resolved
109 down to the small scales of turbulent mixing. The fraction of the spectrum resolved depends on
110 the true spectrum (a function of χ and ε), the flowspeed past the sensor (u), and the response of
111 the thermistor. The GE/Thermometrics FP07 thermistors we use typically resolve frequencies up
112 to about $f_{max} = 10 - 15$ Hz. The maximum resolved wavenumber is then equal to $k_{max} = f_{max}/u$,
113 while the wavenumber extent of the true spectrum varies with k_b (and $\varepsilon^{1/4}$). At the typical vertical
114 fall rate of a CTD rosette (~ 1 m/s), only about 20% of k_b is resolved at $\varepsilon = 10^{-10} \text{ W kg}^{-1}$ (Figure
115 2). While methods have been developed to fit the observed temperature gradient spectrum to
116 theoretical forms (Ruddick et al. 2000), these work only when a larger fraction of the temperature
117 gradient spectrum is resolved. For the relatively high profiling speeds typical of CTD casts, we
118 find these methods do not work well (see appendix for details) and therefore we use the following
119 methodology, which does not have a strongly ε -dependent bias.

120 We first outline our method for estimating χ , which relies on (i) determining the instantaneous
121 flowspeed past the sensor, (ii) identifying periods where the signals may be contaminated by the
122 wake of the CTD rosette, (iii) defining the relevant values of N^2 and $(dT/dz)^2$, and (iv) applying
123 an iterative method to compute χ . We then discuss some limitations and practical considerations
124 that arise.

125 *a. Iterative Method for estimating χ*

126 For each ~ 1 second window, χ is estimated via the following procedure as outlined in Moum
127 and Nash (2009). For isotropic turbulence,

$$\chi_T = 6D_T \int_0^{\infty} \Psi_{T_x}(k) dk \quad (1)$$

128 where D_T is the thermal diffusivity and $\Psi_{T_x}(k)$ is the wavenumber spectrum of dT/dx .

129 Note that dT/dx is not actually measured; dT/dt is measured, and dT/dx is inferred from

130 Taylor's frozen flow hypothesis:

$$\frac{dT}{dx} = \frac{1}{u} \frac{dT}{dt} \quad (2)$$

131 where u represents the flow speed past the sensor. The wavenumber extent of the spectrum depends

132 on the Batchelor wavenumber k_b , which is related to ε :

$$k_b = [\varepsilon / (v D_T^2)]^{1/4} \quad (3)$$

133 We assume that $K_\rho = K_T$ and $K_\rho = \Gamma \varepsilon / N^2$ where Γ is the mixing efficiency, assumed to be 0.2

134 (Moum and Nash 2009). Then dissipation rate is computed as

$$\varepsilon_\chi = \frac{N^2 \chi_T}{2\Gamma \langle dT/dz \rangle^2} \quad (4)$$

135 Typical thermistors do not resolve the spectrum out to k_b , so the measured spectrum is fit to the

136 Kraichnan form of theoretical scalar spectrum over the range of resolved wavenumbers ($k_{min} <$

137 $k < k_{max}$). The variance between the measured $[\Phi_{T_x}(k)]_{obs}$ and theoretical $[\Phi_{T_x}(k)]_{theory}$ spectra at

138 these wavenumbers is assumed to be equal:

$$\int_{k_{min}}^{k_{max}} [\Phi_{T_x}(k)]_{obs} dk = \int_{k_{min}}^{k_{max}} [\Phi_{T_x}(k)]_{theory} dk \quad (5)$$

139 An iterative procedure is then used to fit and calculate χ and ε :

140 1. First we estimate χ_T based on an initial guess of $\varepsilon = 10^{-7}$ Wkg $^{-1}$ and compute k_b via eq. 3.

141 We set $k_{max} = k_b/2$ or to a wavenumber equivalent to $f_{max} = 7$ Hz [i.e., $k_{max} = 2\pi(f_{max})/u$],

142 whichever is smaller. In general f_{max} should be the highest value which is safely below the

143 sensor's roll-off. We chose $f_{max} = 7$ Hz in this case based on inspection of the temperature

144 gradient spectra and historical measurements of these sensors (see appendix for more details).

145 2. We then use Eq. (4) to refine our estimate of ε and k_b and recompute χ_T using Eqs. (1) and
146 (5).

147 3. This sequence is repeated and converges after two or three iterations.

148 Note that this procedure is equivalent to the explicit formulation of (Alford and Pinkel 2000),
149 except we use the Kraichnan theoretical form instead of the Batchelor spectrum for $[\Phi_{T_x}(k)]_{theo}$ 

150 At wavenumbers below the spectral peak, there is little distinction between the Kraichnan and
151 Batchelor spectra, so this factor does not affect the computational bias.

152 *b. CTD- χ pod Data Processing*

153 We next review the basic outline for processing each CTD- χ pod profile. The moored χ pod in-
154 strument (Moum and Nash 2009) has a pressure sensor, compass, and pitot-static tube. In contrast,
155 the CTD- χ pod requires pressure measured by the CTD and has no independent speed measure-
156 ment other than dp/dt from the CTD.

157 1. The correct time-offset for the χ pod clock is determined by aligning highpass-filtered dp/dt
158 from the 24Hz CTD data to integrated vertical accelerations measured by the χ pod. χ pod
159 clock drift is small, typically on the order of 1 sec/week, but it is imperative to get records
160 aligned within < 0.5 s so that the correct value of u is used. In the case of the CTD- χ pod we
161 assume u is solely due to the vertical motion of the CTD cage, i.e. $u = dp/dt$.

162 2. Low-order polynomial calibration coefficients are determined to convert thermistor voltages
163 from χ pod to ITS90 temperature (as measured by the CTD). Figure 3 shows an example of
164 the aligned and calibrated CTD- χ pod timeseries for one cast. Note the significant differences
165 in amount of variance associated with the two sensors during down and up casts. For the
166 upward-mounted sensor (T1), the downcast signal is largely associated with the CTD wake,

as is the upcast for the downward-mounted sensor (T2). Only the ‘clean’ portions of the cast
(e.g., the T1 upcast and the T2 downcast) are used in the χ pod calculations.

3. Depth loops are identified and flagged in the 24Hz CTD data Figure 4. χ pod data during these times are discarded since the signals are likely contaminated by the wake of the CTD. We use a vertical velocity threshold of 0.3m/s and throw out data within 2m of the identified loops. Even for profiles that are significantly affected by ship heaving, good segments of data are obtained over a majority of the depths after removing contaminated data, allowing us to compute values in nearly every 10m bin.

4. Buoyancy frequency N^2 and temperature gradient dT/dz are computed from 1-m binned CTD data, and averaged over a scale of 10m. The results are not very sensitive to the averaging interval (see appendix for more details).

5. Half-overlapping 1 sec windows of data are used to estimate χ and K_T following the methods described in Moum and Nash (2009), as outlined in the previous section.

180 c. Example Spectra and Fits

181 Examples of the observed and fit spectra are shown in Figure 5, for low and high dissipation
182 rate. Note that at lower ε , a larger fraction of k_b is observed and the peak of the spectrum is almost
183 resolved. At higher ε , less of the spectrum is resolved and the spectral peak is well above the
184 maximum resolved wavenumber. Even so, the iterative χ pod method gives an accurate estimate
185 of χ . The χ pod and Chameleon fits are performed over the same wavenumber range and match
186 there. However, the higher-wavenumber protions of the fit spectra differ since the Chameleon fits
187 use the observed k_b to determine the wavenumber extent.

188 **4. Results**

189 *a. Direct Test of χ pod Method*

190 We begin by utilizing the highly-resolved data from the freely-falling turbulence profiler,
191 Chameleon (for which both ε and χ are measured) to test the assumptions in our method of
192 estimating χ . We first apply the χ pod method to each Chameleon profile, using only the FP07
193 thermistor data. These results, which we refer to as χ_{χ}^{cham} and assume no independent knowledge
194 of ε , are then compared to $\chi_{\varepsilon}^{cham}$, computed by integrating the theoretical temperature gradient
195 spectrum where k_b is computed directly from shear-probe derived ε . Qualitatively, χ_{χ}^{cham} and
196 $\chi_{\varepsilon}^{cham}$ show very similar depth and time patterns (Figure 6) and appear to agree in magnitude. A
197 more quantitative comparison (Figure 7), shows the two are well-correlated over five orders of
198 magnitude. The distribution of \log_{10} of the χ ratios is approximately normal, with a mean of
199 $\mu = -0.1$ and standard deviation of $\sigma = 0.51$. This indicates a low bias of χ_{χ}^{cham} relative to $\chi_{\varepsilon}^{cham}$
200 of 20% and random variation of a factor of 3.



201 *b. CTD χ pod - Chameleon Comparison*

202 Having demonstrated that the method works using Chameleon data, we now compare χ_{χ}^{ctd} from
203 CTD-mounted χ pods to $\chi_{\varepsilon}^{cham}$. In contrast to the Chameleon data, the CTD is more strongly
204 coupled to the ship, and therefore subject to more vibration, heaving, and artificial turbulence
205 created by the rosette. A total of 35 CTD- χ pod casts were performed, bracketed with Chameleon
206 profiles immediately before and after. We first compare CTD- χ pod profiles to the mean of the
207 two Chameleon profiles bracketing each cast, both averaged in 5m depth bins (Figure 8). The
208 two are correlated, with considerable scatter. A histogram of the log of ratios is approximately
209 normal and has a mean of -0.31 , indicating a possible small negative bias. Since we expect

210 significant natural variability even between adjacent Chameleon profiles, we investigate further
211 to determine if the observed χ pod variability is of a similar magnitude or greater than expected.
212 Scatter plots of before vs. after Chameleon profiles (not shown), typically  separated by about
213 an hour, show a similar level of scatter as the differences between methods, suggesting that the
214 observed differences (Figure 8) can be explained by natural variability in turbulence. This is
215 demonstrated by histograms of the ratio of χ from adjacent casts (Figure 9) which show that the
216 variability between CTD χ pod and Chameleon casts is similar to the natural variability between
217 before/after Chameleon profiles. Profiles from all CTD-Chameleon pairs averaged in time and
218 40m depth bins (Figure 10) overlap within 95% confidence limits at all depths where there exists
219 good data for both. Averages of subsets of these profiles that were clustered in position/time
220 (not shown) also agree well. We conclude that the variability between CTD χ pod and Chameleon
221 profiles is indistinguishable from natural variability in turbulence levels.

222 5. Discussion

223 We have shown that χ can be accurately estimated from χ pods attached to CTD rosettes. The
224 method also estimates ε , but we have not discussed it here since it involves more assumptions
225 and uncertainties. One major assumption is the mixing efficiency Γ . A value of 0.2 is commonly
226 assumed, but evidence suggests this may vary significantly. Moum and Nash (2009) found a bias
227 of up to 1.6 for Γ values ranging from 0.1 to 0.35. Another major assumption in the χ pod method
228 is that $K_T = K_P$. 

229 The goal of CTD- χ pods is to expand the number and spatial coverage of ocean mixing obser-
230 vations. We have already deployed instruments during several process experiments and on several
231 GO-SHIP repeat-hydrography cruises. We plan to continue regular deployment on GO-SHIP and
232 similar cruises, adding χ to the suite of variables regularly measured. The expanding database of


233 mixing measurements from CTD- χ pods will also enable testing of other commonly-used or new
234 mixing parameterizations. This has the potential to be transformative for the field, allowing the
235 community to develop and test global turbulence parameterizations, use estimates of turbulence
236 along with the CLIVAR repeat hydrography data for inverse models and water mass modification
237 calculations, identify hotspots of turbulence to target with future process experiments, and com-
238 pare with in-situ chemical and biological measurements made routinely on repeat hydrography
239 cruises.



240 6. Conclusions

- 241 • The χ pod method for estimating χ was directly applied to temperature gradients measured
242 by the Chameleon microstructure profiler on > 2700 profiles during the EQ14 cruise. The
243 estimated χ_χ agrees well with χ_ε calculated using ε from shear probes over a wide range of
244 magnitudes (Figure 7) with little or no bias, demonstrating that the method works.
- 245 • CTD- χ pod profiles were also compared to nearby Chameleon profiles during the cruise. Vari-
246 ability between CTD- χ pod and Chameleon estimates of χ is indistinguishable from natural
247 variability between Chameleon profiles. Time-averaged profiles of χ from both platforms
248 agree within 95% confidence limits, and no significant bias was detected between the esti-
249 mates of χ .
- 250 • We conclude that estimates of χ made from the CTD- χ pod platform are robust and reliable.

251 *Acknowledgments.* The EQ14 experiment was funded by budget (NSF?) 1256620. We thank the
252 Captain and crew of R/V Oceanus. Pavana Vutukur, Craig Van Appledorn, Mike Neeley-Brown
253 made the sensors. Aurelie Moulin, Ryan Holmes, Sally Warner and Anna Savage helped to collect
254 the data.

Sensitivity Analysis257 **A1. Flowspeed Past Sensor**

258 To quantify the potential error in the χ calculations from ignoring horizontal velocities
 259 and assuming the flow speed is equal to the vertical speed of the CTD rosette, we repeated the
 260 calculations with constant offsets added to the flowspeed. Note that since the total magnitude of
 261 velocity is used, dp/dt is a minimum estimate of the true speed. Adding 0.1(1)m/s results in a
 262 mean percent error of 14(58) percent (Figure 11), small compared the large natural variability in
 263 turbulence and uncertainty in our measurements. Note that increasing the velocity tends to result
 264 in smaller values of χ , since it shifts the spectrum to lower wavenumbers.

265 We also looked for any systematic biases associated with flowpseed. We found the χ was biased
 266 high for very small speeds ($u < 25\text{cm/s}$). This could be assoicated with contamination by CTD
 267 wake or entrained water when the CTD slows. These values were discarded for our analysis.

268 **A2. N^2 and dT/dz**

269 We investigated the sensitivity of the calculations to the scale over which N^2 , dT/dz are aver-
 270 aged. The iterative method to estimate chi requires the background stratification N^2 and tempera-
 271 ture gradient dT/dz . The estimate of χ is insenstive to these scales. However, while dissipation
 272 rate ε and diffusivity K_T are more strongly affected because they are linearly related to these val-
 273 ues. Computing N^2 and dT/dz over smaller scales (less than a few m) results in larger values and
 274 hence some larger values of K_T .

276

Test of MLE fitting method

277 We also tested the spectrum fitting method of Ruddick et al. (2000) and compared to our χ_{pod}
 278 method. The MLE method works well and gives similar results to our method at true ϵ values
 279 less than about 10^{-9} , but severely underestimates χ at larger values of epsilon, where only a small
 280 fraction of the spectrum is resolved (Figure 12). At lower profiling speeds we would expect the
 281 MLE method to work better, as more of the spectrum will be resolved for a given value of ϵ .

282

APPENDIX C

283

Thermistor Frequency Response

284 Prior to 2009, the transfer function for each FP07 thermistor was measured by profiling adjacent
 285 to a thermocouple in Yaquina Bay, OR. However, measuring the transfer function for each indi-
 286 vidual thermistor proved too expensive and time-consuming, and since that time a generic transfer
 287 function has been used. Figure 13 shows the measured transfer functions for 2008. The majority
 288 of the transfer functions are similar for frequencies up to about 10 Hz, and begin to significantly
 289 differ above that. To estimate the potential error in not using a transfer function, we calculated the
 290 % of spectral variance captured for each of the measured functions. For frequencies up to 7Hz,
 291 more than 95% is captured for 88% of the measured functions. If frequencies up to 15hz are used,
 292 more than 95 % variance is captured only 67% of the time. Using only frequencies up to 7Hz
 293 (where the transfer function is equal to or very close to unity) avoids the issue of the unknown
 294 transfer functions.

295

References

296 Alford, M., and R. Pinkel, 2000: Patterns of turbulent and double diffusive phenomena: Observa-
 297 tions from a rapid profiling conductivity probe. *J. Phys. Oceanogr.*, **30**, 833–854.

- 298 Batchelor, G. K., 1959: Small-scale variation of convected quantitites like temperature in turbulent
299 fluid. *J. Fluid Mech.*, **5**, 113–139.
- 300 Dillon, T. M., 1982: Vertical overturns: A comparison of Thorpe and Ozmidov length scales. *J.*
301 *Geophys. Res.*, **87**, 9601–9613.
- 302 Galbraith, P. S., and D. E. Kelley, 1996: Identifying overturns in CTD profiles. *J. Atmos. Ocean.*
303 *Tech.*, **13**, 688–702.
- 304 Gregg, M., 1989: Scaling turbulent dissipation in the thermocline. *J. Geophys. Res.*, **94** (C7),
305 9686–9698.
- 306 Holmes, R., J. Moum, and L. Thomas, 2016: Evidence for seafloor-intensified mixing by surface-
307 generated equatorial waves. *Geophysical Research Letters*, **43** (3), 1202–1210.
- 308 Kunze, E., E. Firing, J. Hummon, T. K. Chereskin, and A. Thurnherr, 2006: Global abyssal mixing
309 inferred from lowered ADCP shear and CTD strain profiles. *Journal of Physical Oceanography*,
310 **36** (8), 1553–1576.
- 311 Mater, B. D., S. K. Venayagamoorthy, L. S. Laurent, and J. N. Moum, 2015: Biases in Thorpe scale
312 estimates of turbulence dissipation Part I: Assessments from large-scale overturns in oceano-
313 graphic data. *J. Phys. Oceanogr.*, **45** (2015), 2497–2521.
- 314 Melet, A., R. Hallberg, S. Legg, and K. L. Polzin, 2013: Sensitivity of the ocean state to the
315 vertical distribution of internal-tide-driven mixing. *J. Phys. Oceanogr.*, **43** (3), 602–615, doi:
316 <http://dx.doi.org/10.1175/JPO-D-12-055.1>.
- 317 Moum, J., and J. Nash, 2009: Mixing measurements on an equatorial ocean mooring. *J. Atmos.*
318 *Ocean. Tech.*, **26**, 317–336.

- 319 Moum, J. N., 2015: Ocean speed and turbulence measurements using pitot-static tubes on moor-
320 ings. *Journal of Atmospheric and Oceanic Technology*, **(2015)**.
- 321 Munk, W., and C. Wunsch, 1998: Abyssal recipes II: energetics of tidal and wind mixing. *Deep-*
322 *Sea Res. Part I*, **45**, 1977–2010.
- 323 Munk, W. H., 1966: Abyssal recipes. *Deep-Sea Res.*, **13**, 707–730.
- 324 Osborn, T. R., 1980: Estimates of the local rate of vertical diffusion from dissipation measure-
325 ments. *J. Phys. Oceanogr.*, **10**, 83–89.
- 326 Osborn, T. R., and C. S. Cox, 1972: Oceanic fine structure. *Geophys. Fluid Dyn.*, **3**, 321–345.
- 327 Polzin, K. L., A. C. Naveira Garabato, T. N. Huussen, B. M. Sloyan, and S. N. Waterman, 2013:
328 Finescale parameterizations of turbulent dissipation. *Rev. Geophys.*, **submitted**.
- 329 Ruddick, B., A. Anis, and K. Thompson, 2000: Maximum likelihood spectral fitting: The Batch-
330 elor spectrum. *J. Atmos. Ocean. Tech.*, **17**, 1541–1555.
- 331 Scotti, A., 2015: Biases in Thorpe scale estimates of turbulence dissipation Part II: Energetics
332 arguments and turbulence simulations. *J. Phys. Oceanogr.*, **45 (2015)**, 2522–2543.
- 333 Thorpe, S., 1977: Turbulence and mixing in a Scottish Loch. *Philos. Trans. R. Soc. London Ser.*
334 *A*, **286**, 125–181.
- 335 Waterhouse, A. F., and Coauthors, 2014: Global patterns of diapycnal mixing from measurements
336 of the turbulent dissipation rate. *J. Phys. Oceanogr.*, **44 (7)**, 1854–1872.
- 337 Waterman, S., A. C. N. Garabato, and K. L. Polzin, 2013: Internal waves and turbulence in the
338 antarctic circumpolar current. *Journal of Physical Oceanography*, **43 (2)**, 259–282.

- 339 Whalen, C. B., J. A. MacKinnon, L. D. Talley, and A. F. Waterhouse, 2015: Estimating the
340 mean diapycnal mixing using a finescale strain parameterization. *Journal of Physical Oceanog-*
341 *raphy*, **45** (4), 1174–1188, doi:10.1175/JPO-D-14-0167.1, URL <http://dx.doi.org/10.1175/JPO-D-14-0167.1>.
- 343 Whalen, C. B., L. D. Talley, and J. A. MacKinnon, 2012: Spatial and temporal variabil-
344 ity of global ocean mixing inferred from argo profiles. *Geophys. Res. Lett.*, **39** (L18612),
345 doi:10.1029/2012GL053196.

346 LIST OF FIGURES

347	Fig. 1. Photo of CTD rosette during EQ14 with χ pods attached.	21
348	Fig. 2. Ratio of the maximum observed wavenumber $k_{max} = f_{max}/u$ to the Batchelor wavenumber 349 k_b for different values of ϵ , assuming a $f_{max} = 7\text{Hz}$. Each line is for a different flowspeed.	22
350	Fig. 3. Example timeseries from one CTD cast during EQ14. a) CTD pressure. b) Fallspeed of 351 CTD (dp/dt) .c) Vertical and horizontal accelerations measured by χ pod. d) Temperature 352 from CTD and (calibrated) χ pod sensors. T2 is offset slightly for visualization. e) Temper- 353 ature derivative dT/dt measured by the upward-looking χ pod sensor T1. f) Temperature 354 derivative dT/dt measured by the downward-looking χ pod sensor T2.	23
355	Fig. 4. Portion of a CTD cast showing depth vs time (top) for a portion of an upcast, with data 356 flagged as loops in red. Lower panel shows corresponding χ pod timeseries of dT/dt for 357 that time with discarded loop data in red. Note that variance tends to be larger during depth 358 loops due to entrained water and CTD-induced turbulence.	24
359	Fig. 5. Example temperature gradient spectra from EQ14, for high (top) and low (bottom) ϵ . Solid 360 black line with circles show the observed spectra. Dashed line shows the fitted theoretical 361 Kraichnan spectra for the χ pod estimates. Magenta line is Kraichnan spectra for Chameleon 362 χ and ϵ measured at the same depth. Vertical dashed blue(red) lines indicate the minimum 363 (maximum) wavenumber used in the χ pod calculation. The Batchelor wavenumber k_b is 364 also indicated by the vertical cyan line.	25
365	Fig. 6. Depth-time plots of $\log_{10}\chi$ from both methods for EQ14 data. Top: χ pod method. Black 366 diamonds indicate casts used for comparison with CTD- χ pod profiles. Bottom: Chameleon.	26
367	Fig. 7. Left: 2D histogram of $\log_{10}(\chi)$ from Chameleon (x-axis) and χ pod method (y-axes). Values 368 from each profile were averaged in the same 5m depth bins. Right: Normalized histogram 369 of $\log_{10}[\chi_\chi/\chi_\epsilon]$. Vertical dashed line indicates the mean of the the distribution.	27
370	Fig. 8. Left: Scatter plot of χ from CTD- χ pod profiles versus the mean of bracketing Chameleon 371 profiles. Black dashed line shows 1:1, red are $\pm 10\chi$. Right: Normalized histogram of the 372 log of ratios.	28
373	Fig. 9. Histogram of \log_{10} of the ratio of χ for nearby casts. The first set is for the before 374 (cham1) and after (cham2) Chameleon profiles. the 2nd is CTD- χ pod profiles versus the 375 before(cham1) profiles. The last is CTD- χ pod profiles versus the after(cham2) profiles. 376 Dashed lines show the medians of each set. Note that bias is small/zero, and the variability 377 (spread) between CTD/cham is similar to the natural variability between cham profiles.	29
378	Fig. 10. Time mean of χ for all CTD- χ pod - Chameleon cast pairs, with 95% bootstrap confidence 379 intervals.	30
380	Fig. 11. Histogram of % error for χ computed with constant added to fallspeed, in order to examine 381 sensitivity to fallspeed.	31
382	Fig. 12. Left: 2D histograms of χ computed using the interative χ pod method (top) and the MLE fit 383 (bottom) versus χ computed from Chameleon. Note that the MLE method underestimates 384 χ at larger magnitudes. Right: Histograms of the log of ratios for different ranges of ϵ	32

33

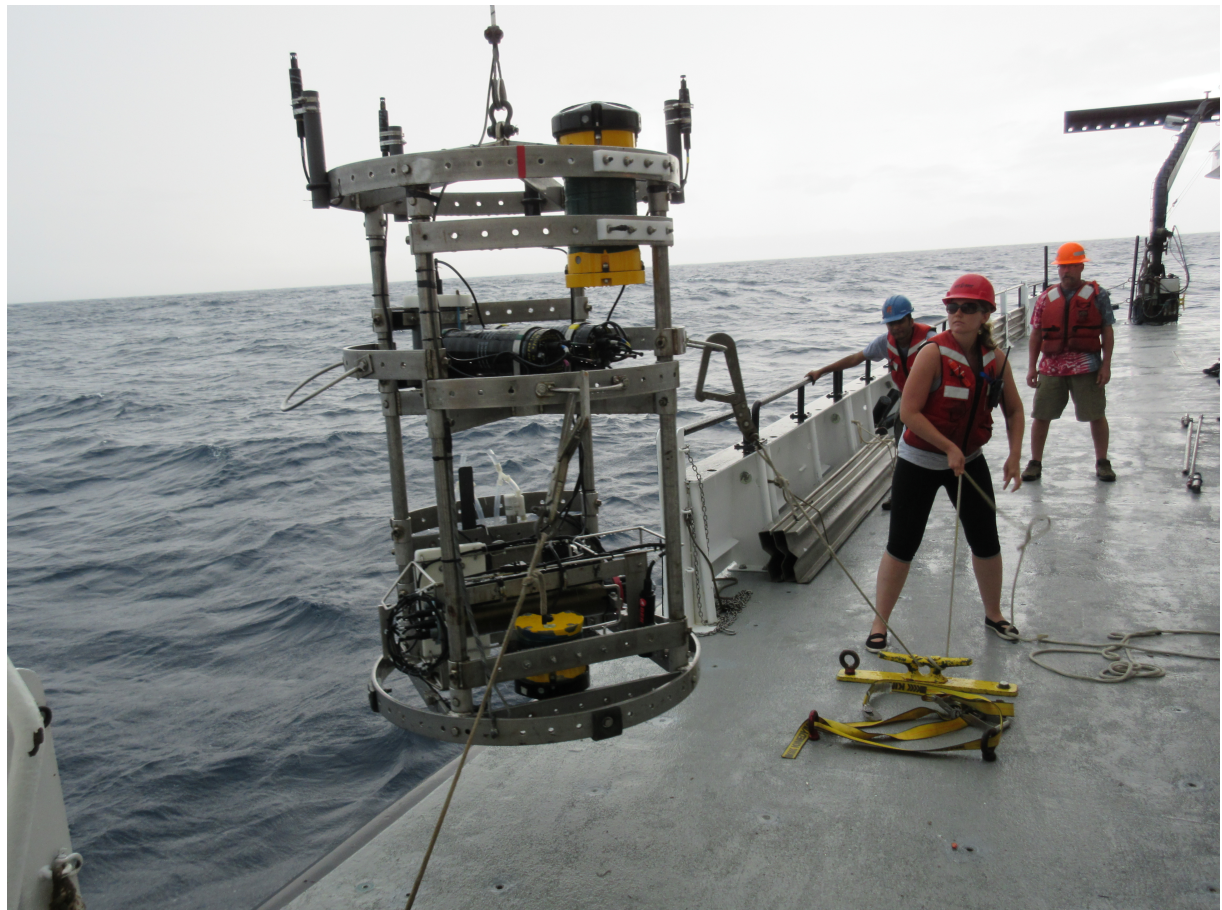
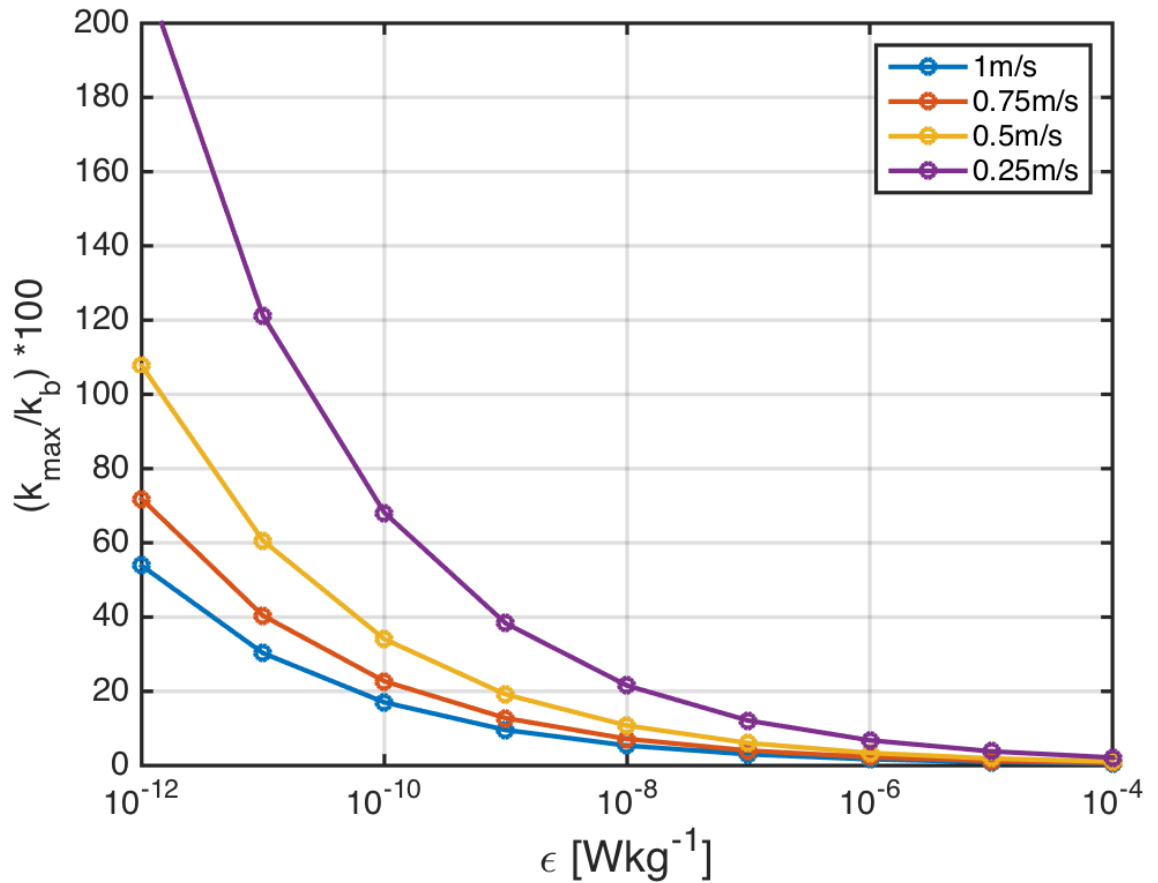
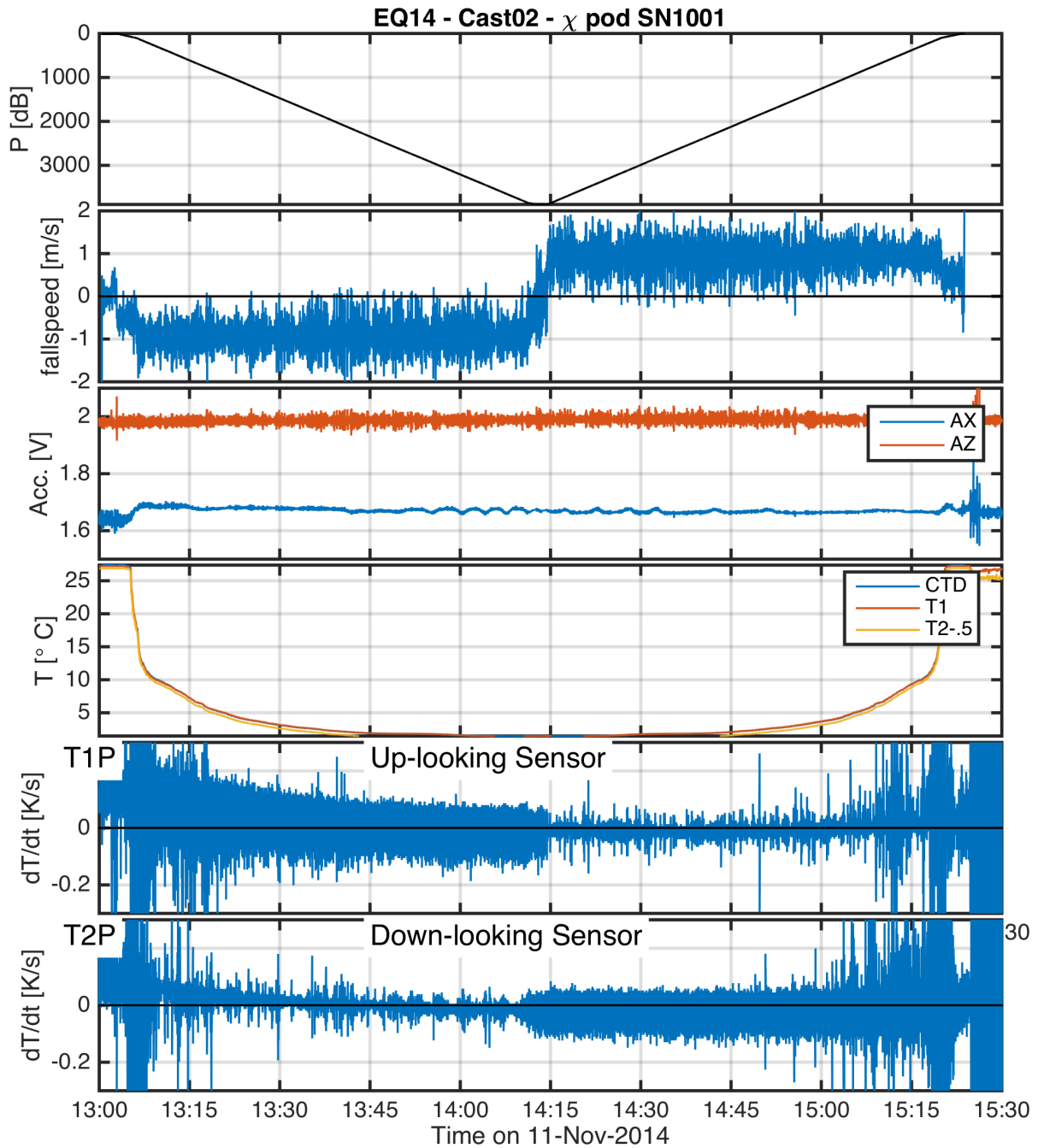


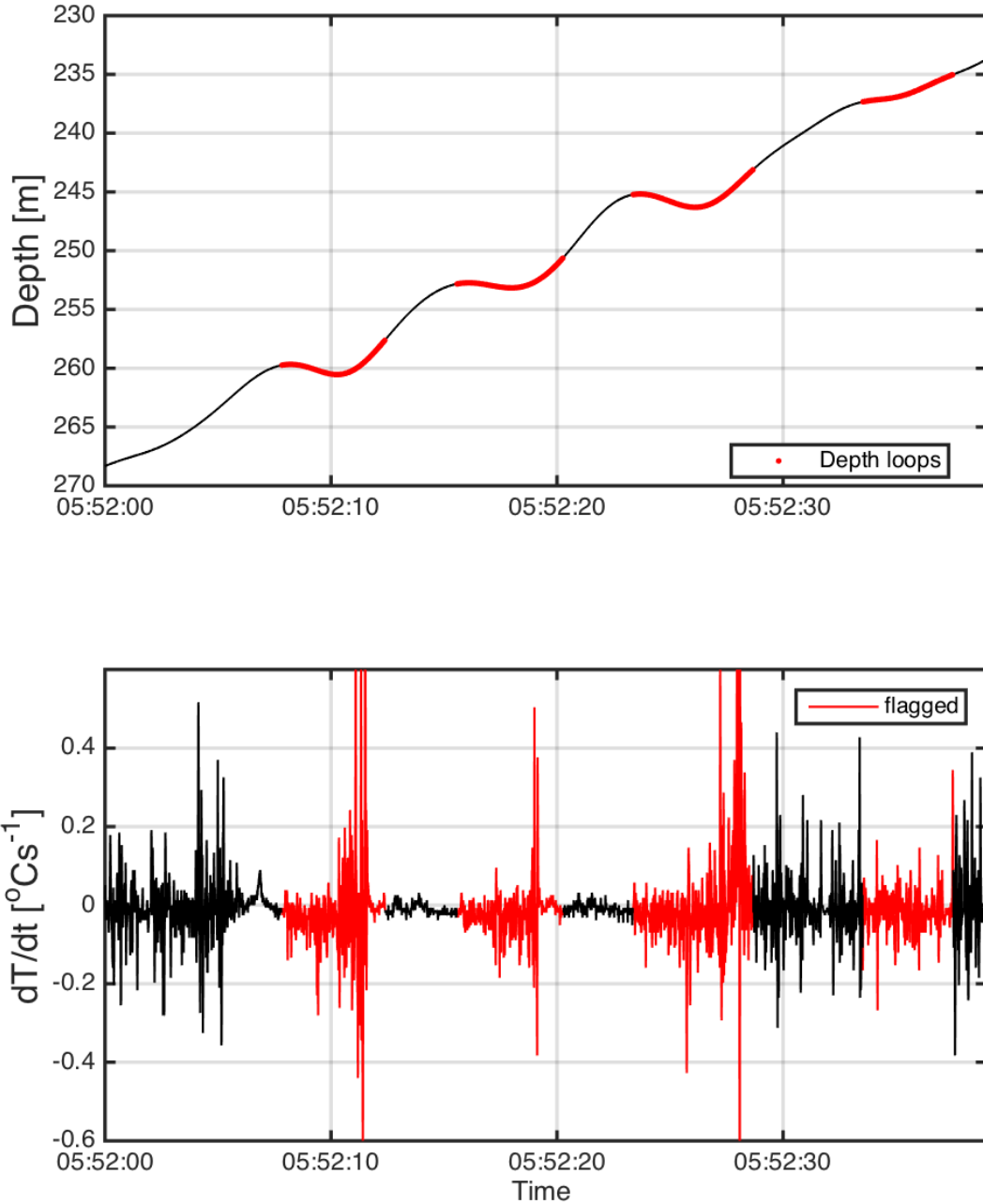
FIG. 1. Photo of CTD rosette during EQ14 with χ pods attached.



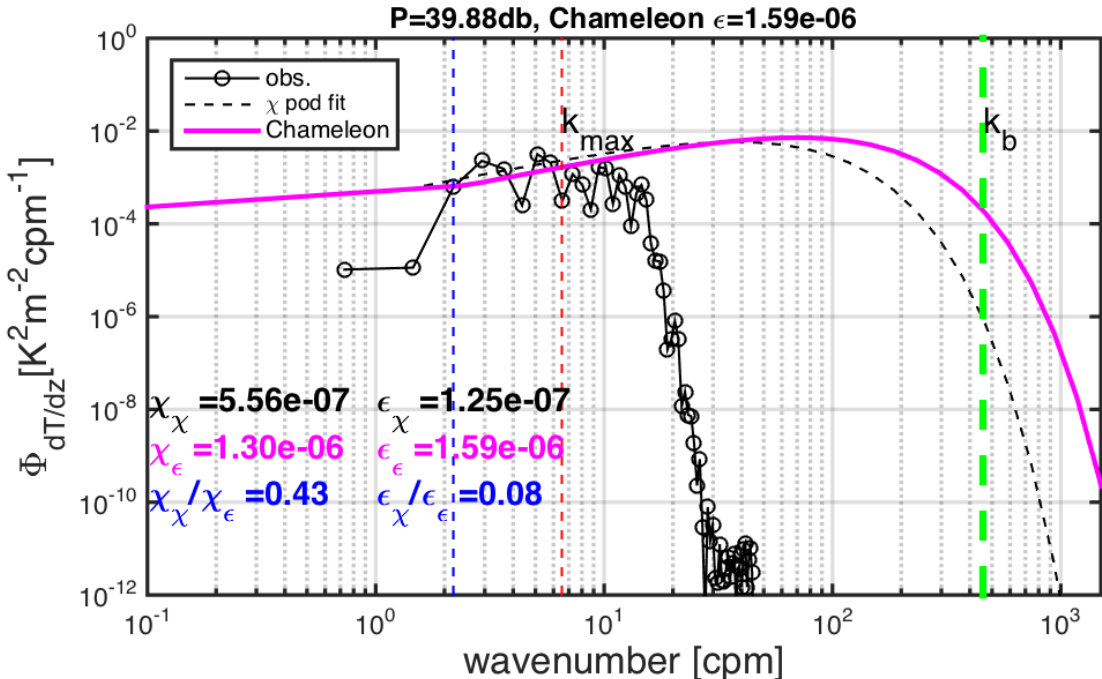
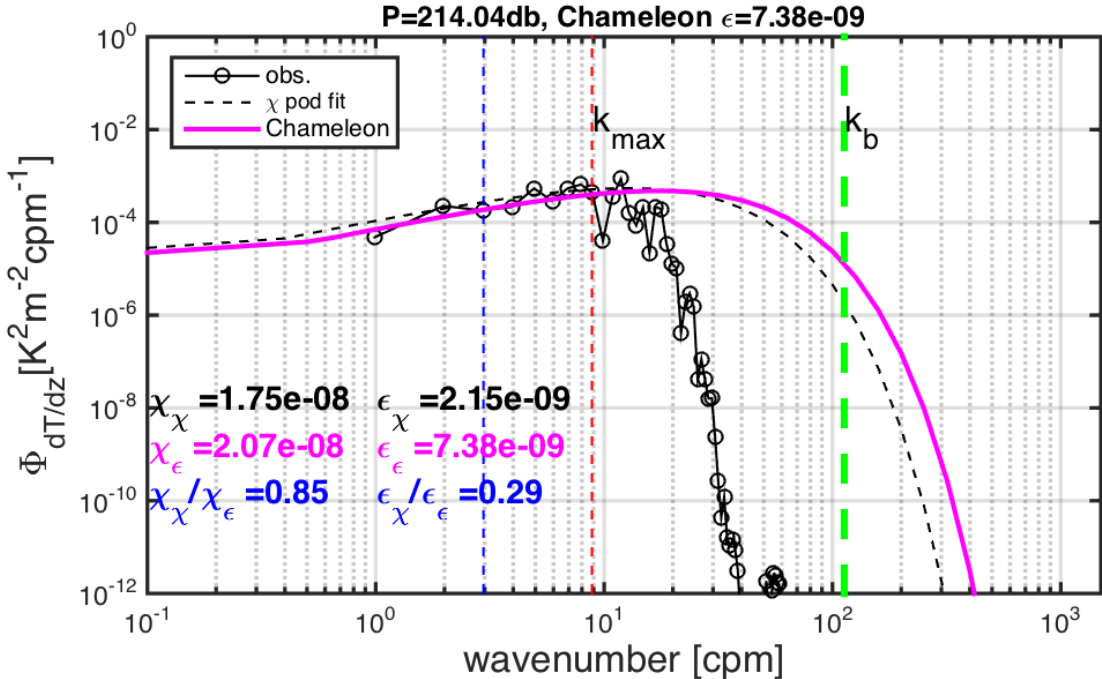
389 FIG. 2. Ratio of the maximum observed wavenumber $k_{\max} = f_{\max}/u$ to the Bachelor wavenumber k_b for
 390 different values of ϵ , assuming a $f_{\max} = 7\text{Hz}$. Each line is for a different flowspeed.



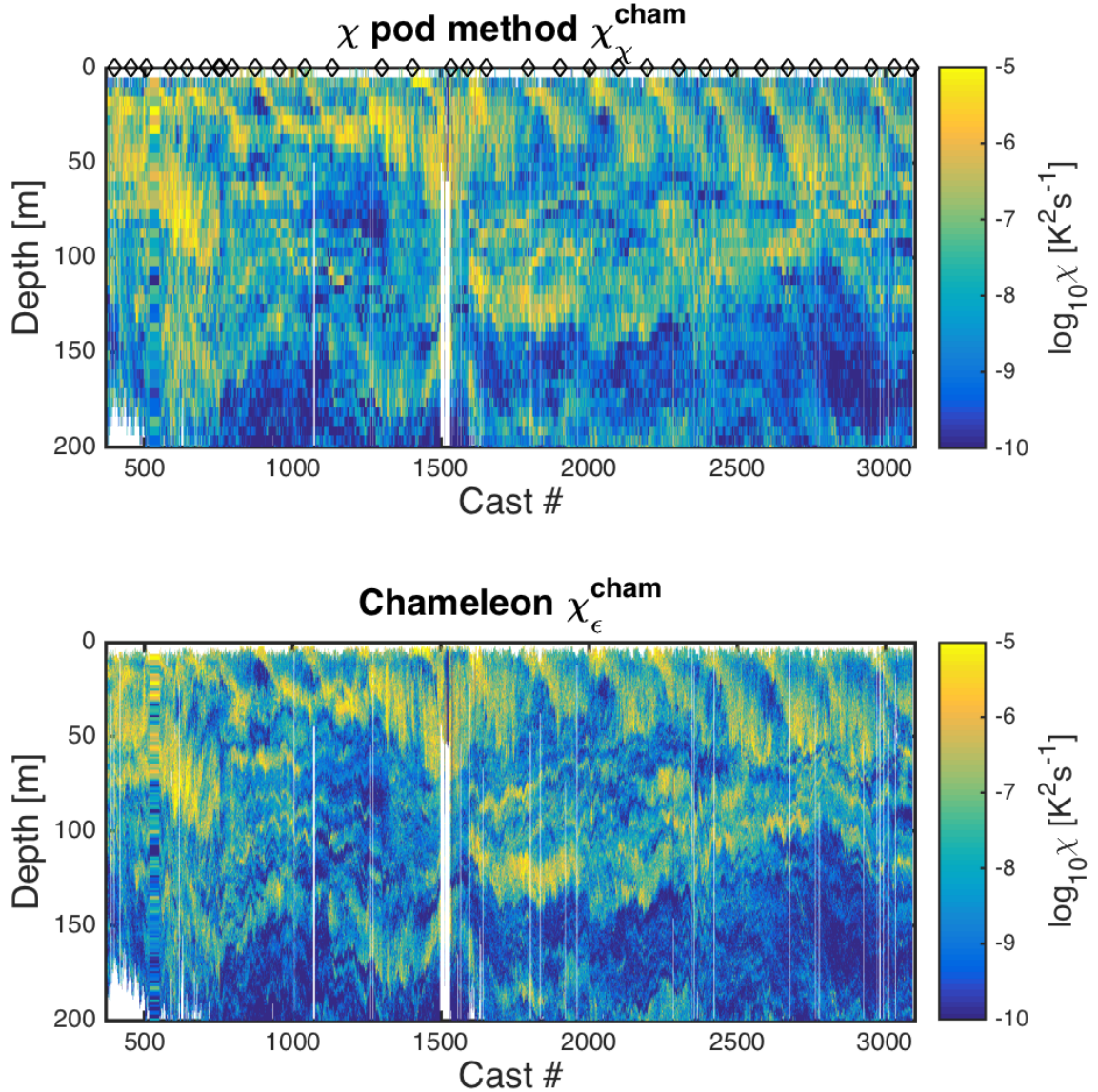
391 FIG. 3. Example timeseries from one CTD cast during EQ14. a) CTD pressure. b) Fallspeed of CTD (dp/dt)
 392 .c) Vertical and horizontal accelerations measured by χ pod. d) Temperature from CTD and (calibrated) χ pod
 393 sensors. T2 is offset slightly for visualization. e) Temperature derivative dT/dt measured by the upward-looking
 394 χ pod sensor T1. f) Temperature derivative dT/dt measured by the downward-looking χ pod sensor T2.



395 FIG. 4. Portion of a CTD cast showing depth vs time (top) for a portion of an upcast, with data flagged as
 396 loops in red. Lower panel shows corresponding χ_{pod} timeseries of dT/dt for that time with discarded loop
 397 data in red. Note that variance tends to be larger during depth loops due to entrained water and CTD-induced
 398 turbulence.



399 FIG. 5. Example temperature gradient spectra from EQ14, for high (top) and low (bottom) ϵ . Solid black
400 line with circles show the observed spectra. Dashed line shows the fitted theoretical Kraichnan spectra for
401 the χ_{pod} estimates. Magenta line is Kraichnan spectra for Chameleon χ and ϵ measured at the same depth.
402 Vertical dashed blue(red) lines indicate the minimum (maximum) wavenumber used in the χ_{pod} calculation.
403 The Batchelor wavenumber k_b is also indicated by the vertical cyan line.



404 FIG. 6. Depth-time plots of $\log_{10}\chi$ from both methods for EQ14 data. Top: χ pod method. Black diamonds
 405 indicate casts used for comparison with CTD- χ pod profiles. Bottom: Chameleon.

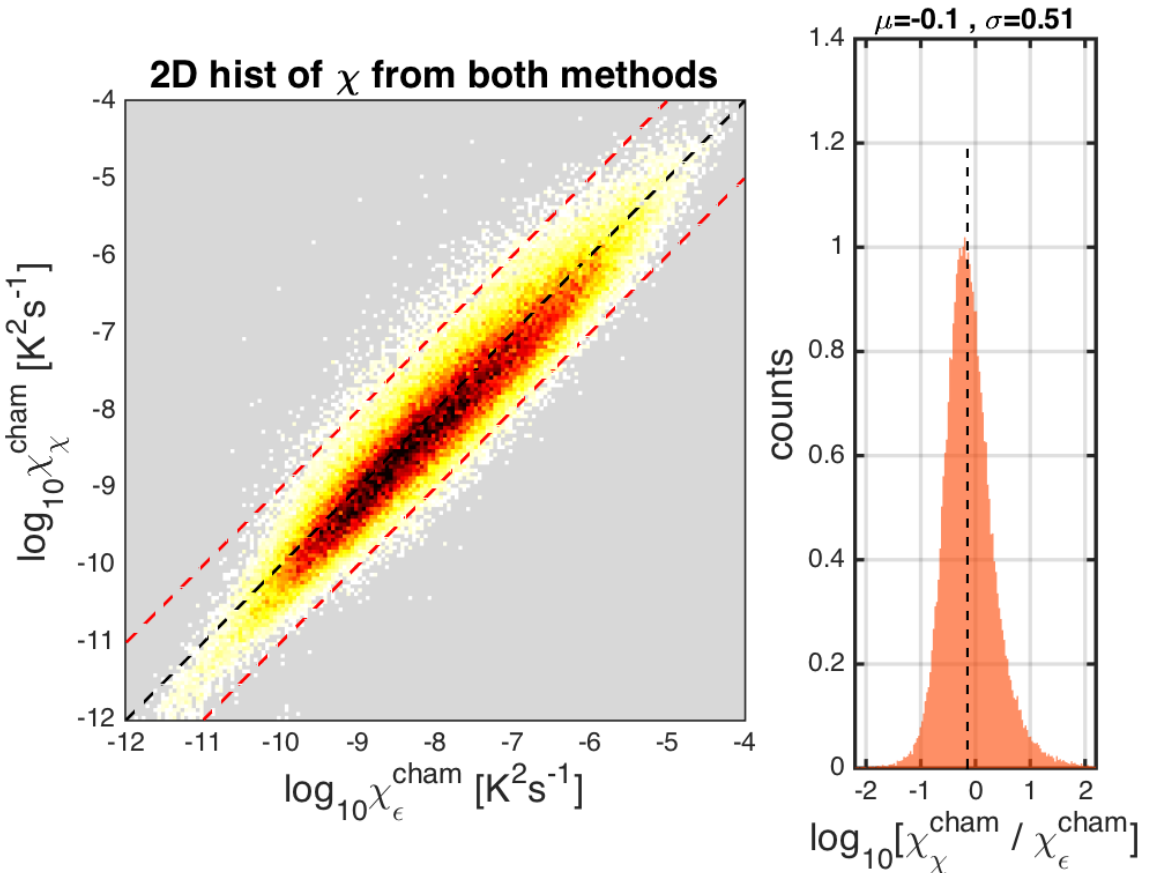


FIG. 7. Left: 2D histogram of $\log_{10}(\chi)$ from Chameleon (x-axis) and χ_{pod} method (y-axes). Values from each profile were averaged in the same 5m depth bins. Right: Normalized histogram of $\log_{10}[\chi_{\chi}/\chi_{\epsilon}]$. Vertical dashed line indicates the mean of the the distribution.

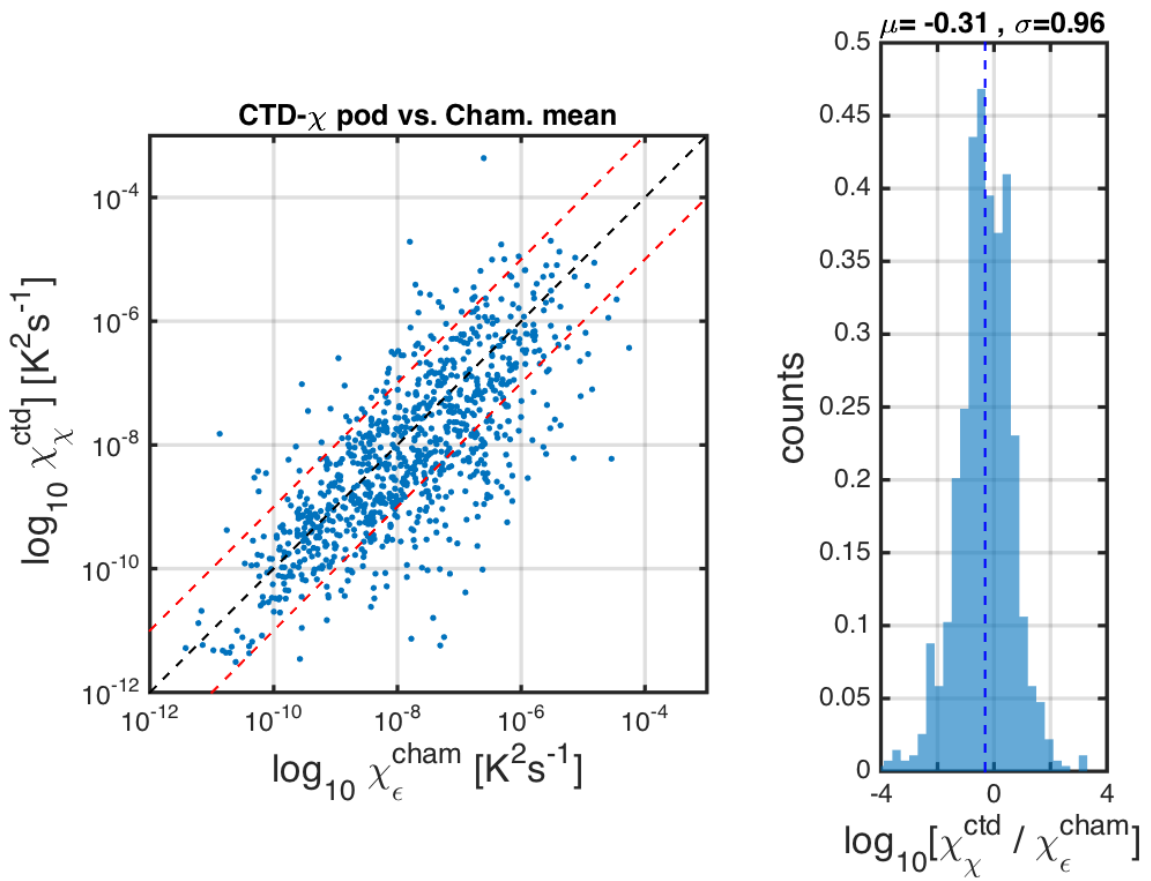
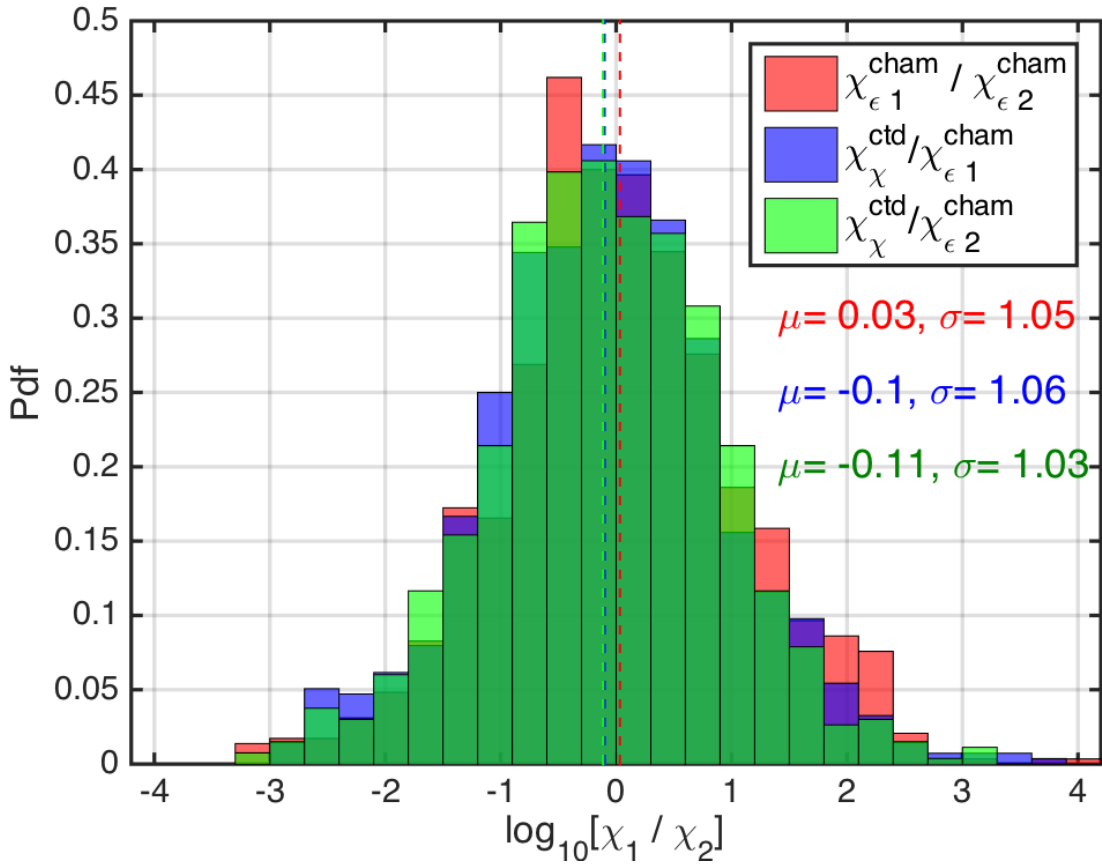


FIG. 8. Left: Scatter plot of χ from CTD- χ pod profiles versus the mean of bracketing Chameleon profiles.
 409
 410 Black dashed line shows 1:1, red are ± 10 X. Right: Normalized histogram of the log of ratios.



411 FIG. 9. Histogram of \log_{10} of the ratio of χ for nearby casts. The first set is for the before (cham1) and
 412 after (cham2) Chameleon profiles. the 2nd is CTD- χ pod profiles versus the before(cham1) profiles. The last is
 413 CTD- χ pod profiles versus the after(cham2) profiles. Dashed lines show the medians of each set. Note that bias
 414 is small/zero, and the variability (spread) between CTD/cham is similar to the natural variability between cham
 415 profiles.

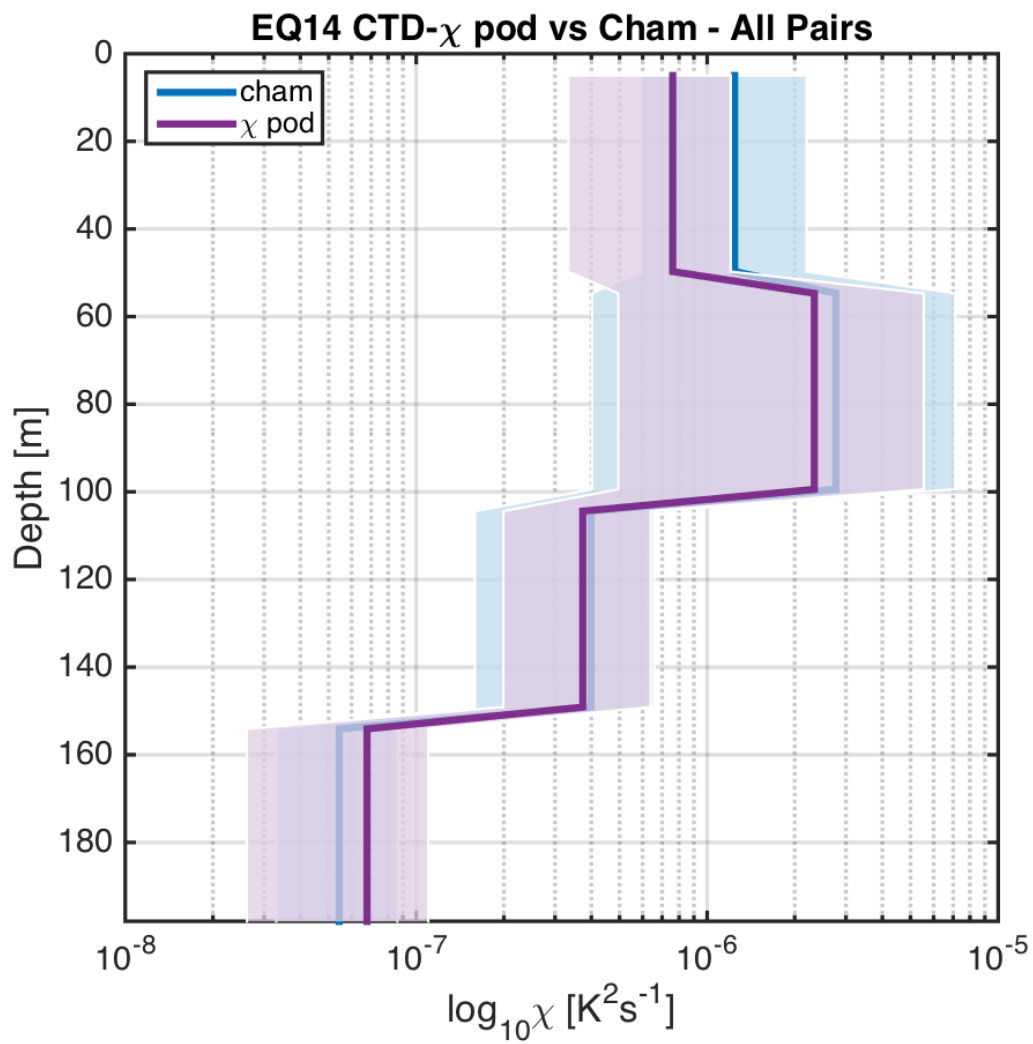
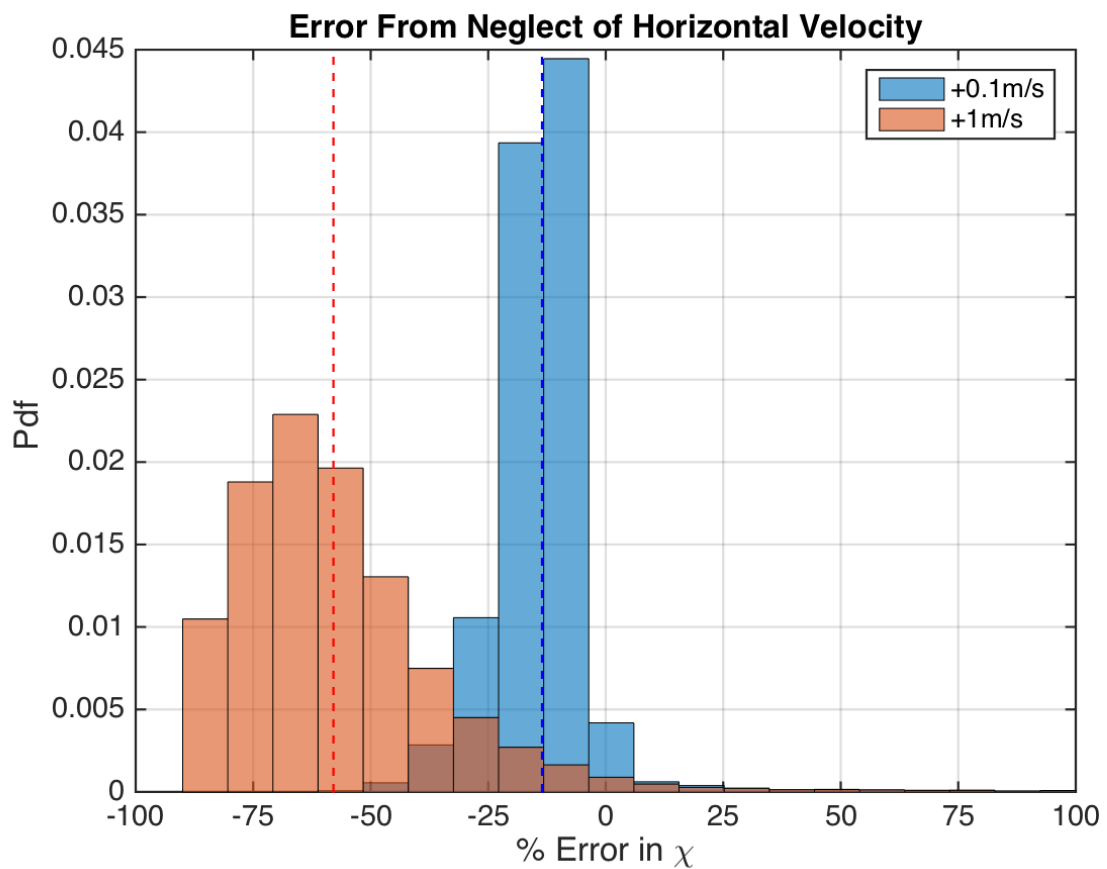


FIG. 10. Time mean of χ for all CTD- χ pod - Chameleon cast pairs, with 95% bootstrap confidence intervals.



⁴¹⁶ FIG. 11. Histogram of % error for χ computed with constant added to fallspeed, in order to examine sensitivity
⁴¹⁷ to fallspeed.

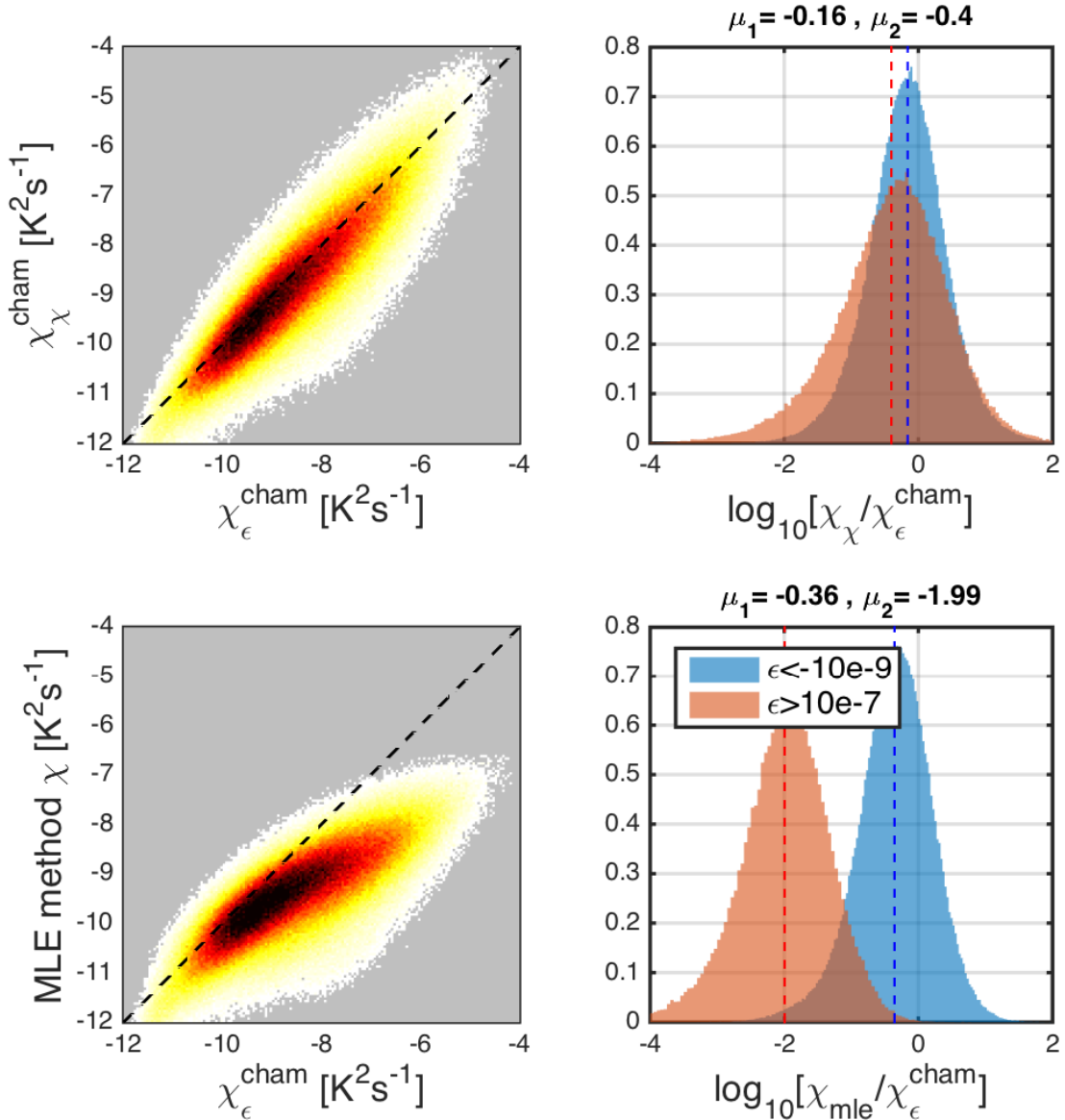
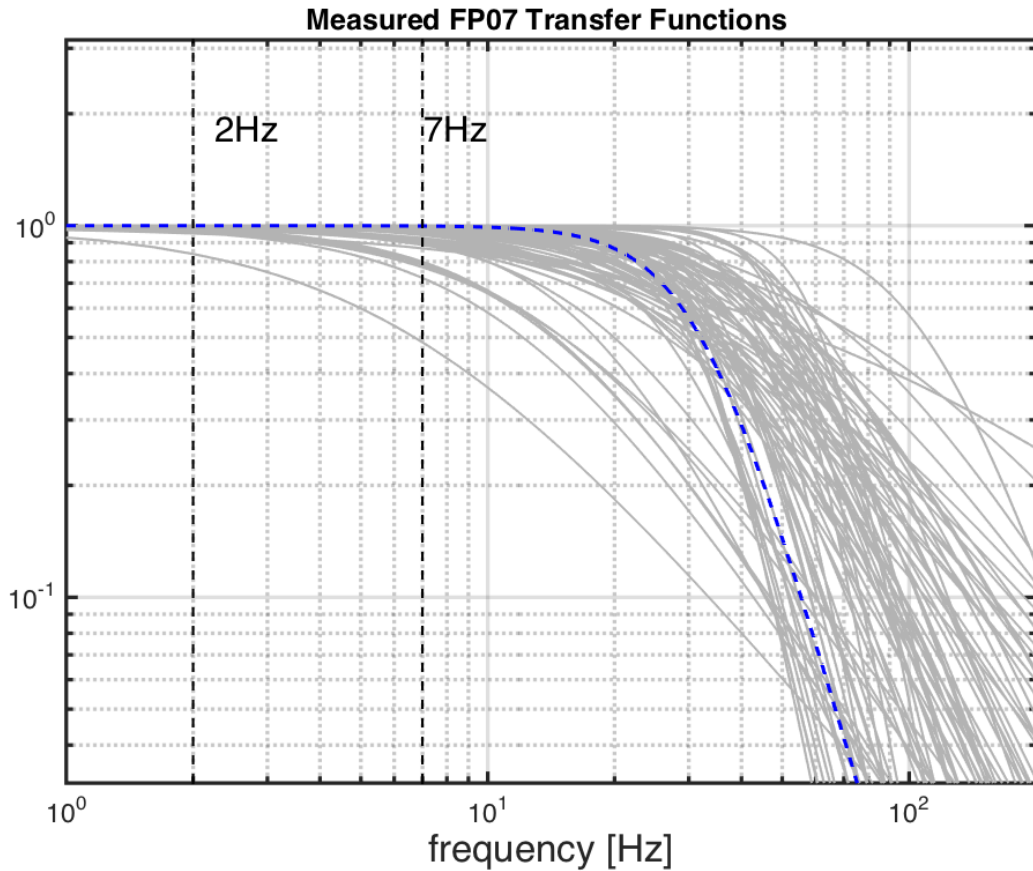


FIG. 12. Left: 2D histograms of χ computed using the interative χ_{pod} method (top) and the MLE fit (bottom) versus χ computed from Chameleon. Note that the MLE method underestimates χ at larger magnitudes. Right: Histograms of the log of ratios for different ranges of ϵ .



421 FIG. 13. Measured FP07 thermistor transfer functions from historical database. Vertical dashed lines show
 422 the frequency range used in χ pod method. Dashed blue line is a generic transfer function found to best match
 423 measured functions, and is used when response functions are no longer measured.